GPS Solutions (2018) 22:116
https://doi.org/10.1007/s10291-018-0781-3

ORIGINAL ARTICLE

Global coherence of GPS-measured high-frequency surface tremor motions

Alexey Lyubushin[1]

Received: 18 March 2018 / Accepted: 24 August 2018

Abstract
The traditional approach of GPS investigations is determining trends which are connected with the motion of tectonic plates. At the same time, a global GPS network provides the possibility of investigating statistical properties of high-frequency earth surface tremor in different parts of the world. Based on the results of coherence and correlation analysis of noise components of daily three-component GPS time series, representing measurements of earth surface displacements at 1097 stations, we have found that, during 2010–2011, there was a significant increase in the average level of noise coherence or correlation with dominant periods 7–9 days of surface tremor in nine regions of the earth, and in some of these regions, the average level of coherence or correlation is still high and does not return to the previous level. The increase of the average level of coherence and correlation could be detected on the graphs purely visually, while the middle time point of the time interval in which the ascending occurred is detected more precisely by a formal method based on the use of the Fisher's ratio.

Keywords GPS noise · Spectral coherence measure · Correlation · Synchronization · Fisher's ratio

Introduction

The detailed structure of high-frequency components of GPS time series has been an object of investigations for a long time. The most frequently analyzed parameter is the spectral index. Langbein and Johnson (1997) were among the first who classified GPS signals using power laws fitted to spectra and maximum-likelihood approach for estimating amplitudes of different types of noise. In Zhang et al. (1997), the problem of uncertainty in GPS measurements due to the presence of color and flicker noise components is investigated. Mao et al. (1999) investigated the influence of flicker noise on estimating velocity errors in a GPS coordinate time series as a function of latitude. Blewitt and Lavallee (2002) and Bos et al. (2010) estimated the influence of seasonal variations in GPS time series, which occur due to hydrological loading, on the determining of tectonic plates velocity. Caporali (2003) investigated uncertainties of velocity determination in connection to the shape of spectral density and values of the spectral index of GNSS time series. Williams et al. (2004), Bos et al. (2008), and Wang et al. (2012) continued works on estimating white and power-law noise amplitudes in GPS time series from different GPS solution systems and from different regions by applying maximum-likelihood approach. The structure of high-frequency GPS noise in New Zealand and the USA was investigated and compared in Beavan (2005). Teferle et al. (2008) applied empirical orthogonal function analysis for extracting common spatial and temporal features in GPS time series from the network in Europe. Li et al. (2000) analyzed crustal deformations in Central Japan using ARMA parametric models of GPS time series for the purpose of removing white noise components and detecting of data discontinuities to distinguish between the tectonically active and inactive regions. Langbein (2008) studied the spatial distribution of GPS noise properties in California. Bock et al. (2011) suggested a method for joint analysis of high-frequency components of GPS time series and seismic waveforms from a network of broadband accelerometers. In Chen et al. (2013), a method for extracting seasonal components from GPS time series was proposed which is based on applying nonparametric Singular Spectrum Analysis. Hackl et al. (2013) focused their studies on extracting transient effects within noise component of GPS time series for detecting slow-slip events. Software package for analysis of

✉ Alexey Lyubushin
lyubushin@yandex.ru

[1] Institute of Physics of the Earth, Russian Academy of Sciences, Moscow, Russia

Published online: 05 September 2018

different properties of GPS time series includes spectral and wavelet-based statistics proposed in Goudarzi et al. (2013). Khelif et al. (2013) studied positioning stability of stations and noise variance of the GPS time series with the help of a discrete wavelet transform. In Lyubushin and Yakovlev (2016), entropy measure was applied for investigating stepwise components of GPS time series.

We propose the method for investigating GPS noise coherence and correlation based on estimating mean squared by-pair coherence spectra for a large number of daily GPS time series using a two-dimensional vector autoregression model and calculating mean absolute values of all by-pair correlation coefficients. It is applied to GPS signals on a network of stations, covering nine different regions of the world. The analysis is performed for the random fluctuations of signals which are obtained by the transition to increments.

Data

Positions of 1191 GPS stations which have daily time series of 4384 samples ranging from May 10, 2006 to May 11, 2018 (12 years), having a total number of gaps of less than 360 samples, and longest gap of less than 180 samples, are presented at Fig. 1 by red points. Blues lines indicate nine rectangular domains which were extracted for joint processing of daily GPS time series from the stations inside these domains.

These daily GPS time series were downloaded from the site http://gf9.ucs.indiana.edu/daily_rdahmmexec/daily of Indiana University. This site contains large zip files with filenames UNR_IGS08_Year-Month-Day.zip, e.g., UNR_IGS08_2018-06-13.zip of size 3,261,818,674 bytes, which is modified each day. Inside the large zip file, there are 10,590 small zip files which correspond to different permanent stations all over the world; for instance, the file daily_project_00NA_2018-06-13.zip. Abbreviation UNR means that the initial source of the data is University of Nevada, Reno. Each small zip file contains a table of daily GPS time series using model IGS08, including standard deviations and coordinates of the stations. Gaps in the GPS time series are filled by constant values corresponding to the last sample before the gap. We used a different method of filling the gaps using information from the left-hand and right-hand vicinities of the gap of the same length as the length of the gap. The method is described below.

Table 1 contains the parameters of extracted domains. It should be noticed that the domain which is called "Australia" contains stations which are located in Indonesia and China, as well. Thus, some of the domain names are not strictly reflecting the geographical location.

Filling the gaps

In terms of notation, the symbols E, N, and U will be used to denote increments of daily time series of the earth's surface displacements in the east–west, north–south, and vertical directions. In addition, the same symbols will be used to distinguish the different properties of these time series.

Before processing, the gaps were filled using information from right-hand and left-hand neighboring parts of the records having the same length as the length of the gap. The method is very simple and is intended for processing time series with dominant low-frequency components. It consists in filling the gap by half the sum of left-hand and right-hand pieces of the same length as the length of the gap. The main

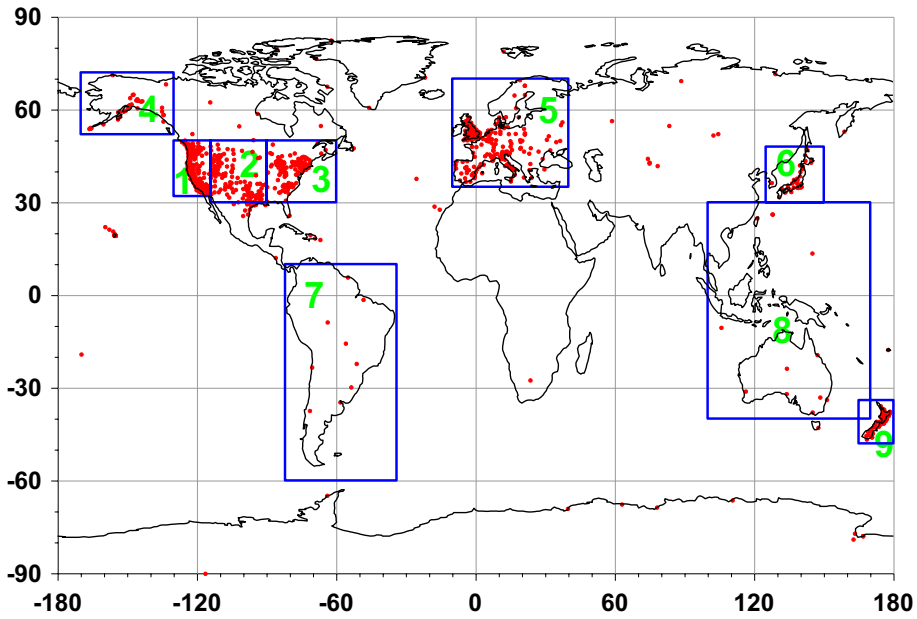

Fig. 1 Station locations and domains. Red points present positions of 1191 GPS stations which have daily records containing 4384 samples and covering the period May 10, 2006–May 11, 2018. The total number of gaps is less than 360 samples. Blue lines indicate nine domains which will be used for the estimation of coherence

Table 1 Parameters of nine domains

#	Domain	Minimum latitude, deg.	Maximum latitude, deg.	Minimum longitude, deg.	Maximum longitude, deg.	Number of stations
1	West USA	32	50	−130	−114	427
2	Middle USA	30	50	−114	−90	161
3	East USA	30	50	−90	−60	153
4	Alaska	52	72	−170	−130	37
5	Europe	35	70	−10	40	209
6	Japan	30	48	125	150	30
7	South America	−60	10	−82	−34	9
8	Australia	−40	30	100	170	12
9	New Zealand	−48	−34	165	180	59

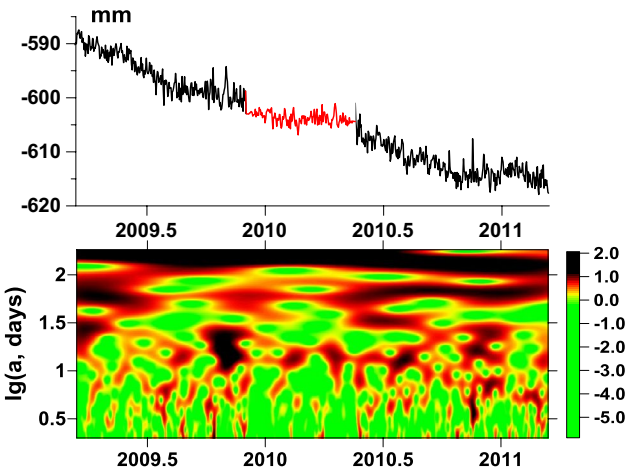

Fig. 2 Example of filling gaps in the daily GPS time series. Fragment of the E-record from station AB50, located at longitude =-134.545, latitude = 58.4168. Top panel: real data [black lines, filled data (red line); length of the gap is 168 days]. Bottom panel: Morlet wavelet diagram of the completed data illustrating the continuity of the time–frequency composition after filling in the missing. The color scale at the bottom panel presents values of logarithm of squared wavelet coefficients which could be interpreted as logarithm of energy of oscillations at the vicinity of certain time point with period a

goal of such filling procedure is preserving the general properties of spectral time–frequency structure inside the gap.

Figure 2 illustrates the result of the filling procedure. Time–frequency diagram at the bottom panel presents the distribution of the logarithm of squared absolute Morlet wavelet coefficients $\lg|c(t,a)|^2$ which are calculated by the convolution of the signal $x(s)$ with Morlet kernel function $\psi(t)$ (Mallat 1999):

$$c(t,a) = \frac{1}{\sqrt{a}} \int_{-\infty}^{+\infty} x(s) \cdot \psi\left(\frac{s-t}{a}\right) \mathrm{d}s, \quad a > 0,$$
$$\psi(t) = \frac{1}{\pi^{1/4}} \exp(-t^2/2 - i\pi t). \tag{1}$$

The values of $|c(t,a)|^2$ could be interpreted as the energy of oscillation of the signal $x(s)$ at the vicinity of time moment t with a period a. The bottom panel shows that the used method of filling gaps provides continuity of time–frequency spectral composition of the signal.

The purpose of our analysis is an investigation of coherence and correlation effects between high-frequency variations of GPS time series from different stations. The simplest way for getting such noise component of the signals is considering their increments, i.e., differences between successive values of time series. Figure 3 presents the graphs of such increments for three components of daily time series for nine GPS stations from the domain South America. It could be noticed that amplitudes of increments for vertical components U are considerably higher than for horizontal E and N. This is the consequence of well-known fact that vertical motion of earth's surface is measured with less accuracy and is characterized by higher noise level (Mao et al. 1999). This fact will be confirmed further on by estimates of mean power spectra (Fig. 5) and mean standard deviations within moving time windows (Fig. 12).

Power spectra of GPS time series

Before investigating the coherence effects of multidimensional GPS time series, let us estimate and look at the shape of their power spectra. Black lines in Fig. 4 present the results of calculating power spectra of 427 time series corresponding to E component from the domain #1 (West USA), whereas green line presents the average of all these spectra.

Let us repeat this operation for all three components and for all nine domains from Table 1. The results are presented as the Fig. 5. The most interesting peculiarity

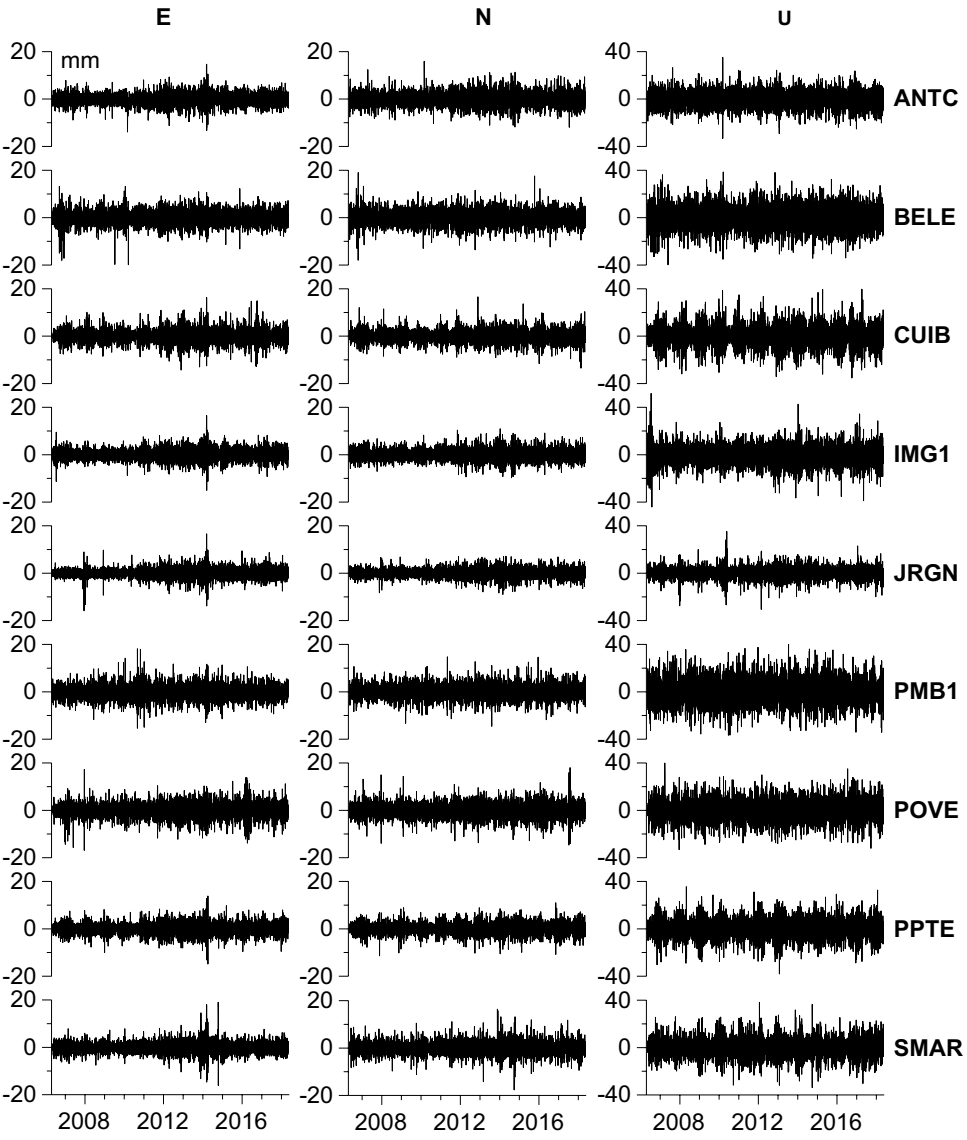

Fig. 3 Graphs of increments of daily time series for nine GPS stations from the domain South America. Station names are shown on the right of each graph. Values of increments are given in millimeters

of this figure is the abnormal behavior of power spectra for E component from domains #6 (Japan) and #7 (South America). Thus, the spectral indexes of averaged spectra of E components from these domains strongly differ for small and large periods. It should be noticed that the E component corresponds to the direction of plate tectonic subduction in the Pacific region. Besides that, Japan is the region of Tohoku mega-earthquake on March 11, 2011, $M = 9.1$, whereas South America is the region of the previous Maule mega-earthquake in Chile on February 27, 2010, $M = 8.8$. In Filatov and Lyubushin (2017), it was shown that large difference between fractal indexes, which are proportional to spectral indexes, of GPS time series for small and large time scales corresponds to seismically dangerous regions.

Mean spectral measure of coherence

We want to construct some spectral measure of mean joint coherence between a large number of time series from each domain. For instance, the number of time series from the domain West USA equals 427. That is why, using multidimensional spectral methods, which are based on estimating spectral matrices, is rather difficult regarding computations and does not provide the robustness of the result. Let us consider squared coherence spectra between

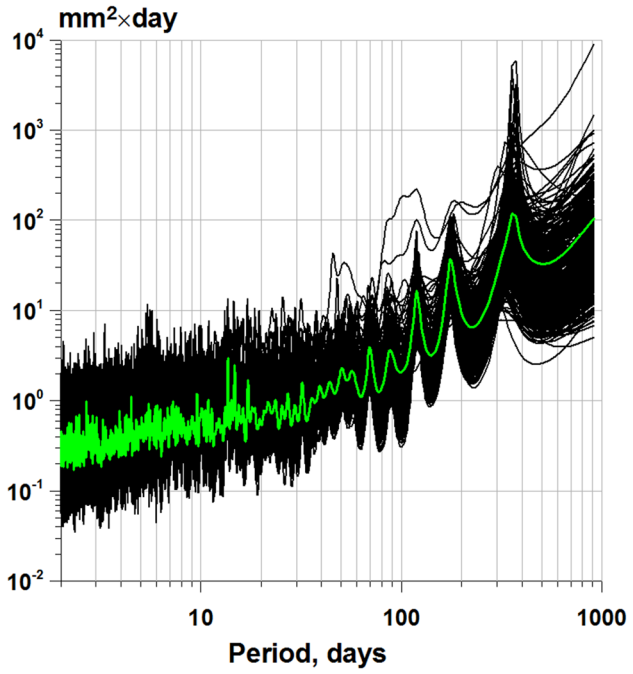

Fig. 4 Graphs of power spectra estimates of E records from domain #1 of the Table 1 (West USA). The green line is the graph of the averaged power spectrum

all different pairs of time series. If the number of time series within a domain equals q, then the number of different pairs equals $q \cdot (q-1)/2$. Let us consider a sliding time window of certain length L samples which is moving with some mutual shift ΔL samples, and let τ be the time corresponding to the right-hand end of moving time window. Let

$$S^{(k,j)}(\tau,\omega) = \begin{pmatrix} S_k(\tau,\omega) & S_{kj}(\tau,\omega) \\ S_{jk}(\tau,\omega) & S_j(\tau,\omega) \end{pmatrix} \tag{2}$$

be a Hermitian spectral matrix of the size 2×2 which is estimated using data from the time window with right-hand end time moment τ, and ω is a frequency value. Here, S_k is the power spectrum of the scalar time series with number $k = 2, ..., q$, S_j is the power spectrum of scalar time series with number $j = 1, ..., (k-1)$, and S_{kj} is complex cross-spectrum between time series k and j, $S_{jk} = S_{kj}^*$.

By-pair squared spectral coherence between time series k and j is calculated by the formula

$$\gamma_{kj}^2(\tau,\omega) = |S_{kj}(\tau,\omega)|^2 \Big/ \big(S_k(\tau,\omega) \cdot S_j(\tau,\omega)\big). \tag{3}$$

It is well known that $0 \le \gamma_{kj}^2(\tau,\omega) \le 1$ and value (3) could be regarded as the frequency-dependent squared correlation coefficient (Marple 1987; Box et al. 2015). The mean spectral measure could be defined by the formula:

$$\varphi(\tau,\omega) = \sum_{k=2}^{q} \sum_{j=1}^{k-1} \gamma_{kj}^2(\tau,\omega)/(q \cdot (q-1)/2). \tag{4}$$

For calculating the mean coherence (3), it is necessary to estimate spectral matrices (2) for all pairs of different scalar time series within each time window. For this purpose, we used a vector autoregression model for m-dimensional time series (in our case, $m = 2$):

$$Z(t|\tau) + \sum_{l=1}^{p} A_l(\tau) \cdot Z(t-l|\tau) = e(t|\tau)\,, \tag{5}$$

where t is time index within current time window with the time coordinate τ, $Z(t|\tau)$ is the piece of m-dimensional time series corresponding to the current time window, p is an autoregression order, $A_l(\tau)$ are matrices of autoregression coefficients of the size $m \times m$, and $e(t|\tau)$ is m-dimensional residual signal with zero mean and covariance matrix $\Phi(\tau) = M\{e(t|\tau)e^T(t|\tau)\}$. Matrices $A_l(\tau)$ and $\Phi(\tau)$ are defined in each time window using Durbin–Levinson procedure (Marple Jr. 1987; Hamilton 1994; Box et al. 2015) and the spectral matrix is calculated using the formula:

$$\begin{aligned} S(\tau,\omega) &= F^{-1}(\tau,\omega) \cdot \Phi(\tau) \cdot F^{-H}(\tau,\omega), \\ F(\tau,\omega) &= E + \sum_{l=1}^{p} A_l(\tau) \cdot \exp(-i\omega l), \end{aligned} \tag{6}$$

where E is a unit matrix of the size $m \times m$ and H is the sign of Hermitian conjunctions.

We applied the model (6) for the case when $m = 2$ within time windows of the length $L = 182$ daily samples (0.5 years) with mutual shift $\Delta L = 28$ samples for time series of increments.

We used autoregression order $p = 5$ in the (5). It is important that, before calculating the spectral matrix, each scalar component of the multidimensional time series was subjected (independently in each time window) to the preliminary operations of winsorizing (Huber and Ronchetti 2009): sample mean and standard deviation σ were iteratively calculated, the mean was subtracted from the sample, after which the counts were divided by σ, and all the values that fell beyond the limits of $\pm 3\sigma$ were replaced by their limiting values. The iterations were repeated until σ stopped changing. These procedures ensure the robustness of the estimate of the coherence measure to the outliers (extreme values).

Figure 6 presents time–frequency diagrams of mean squared coherence for all nine domains and for all three components of GPS time series. It could be noticed that, starting from 2010 to 2011, the mean coherence essentially increases for all domains, especially for the horizontal components E and N.

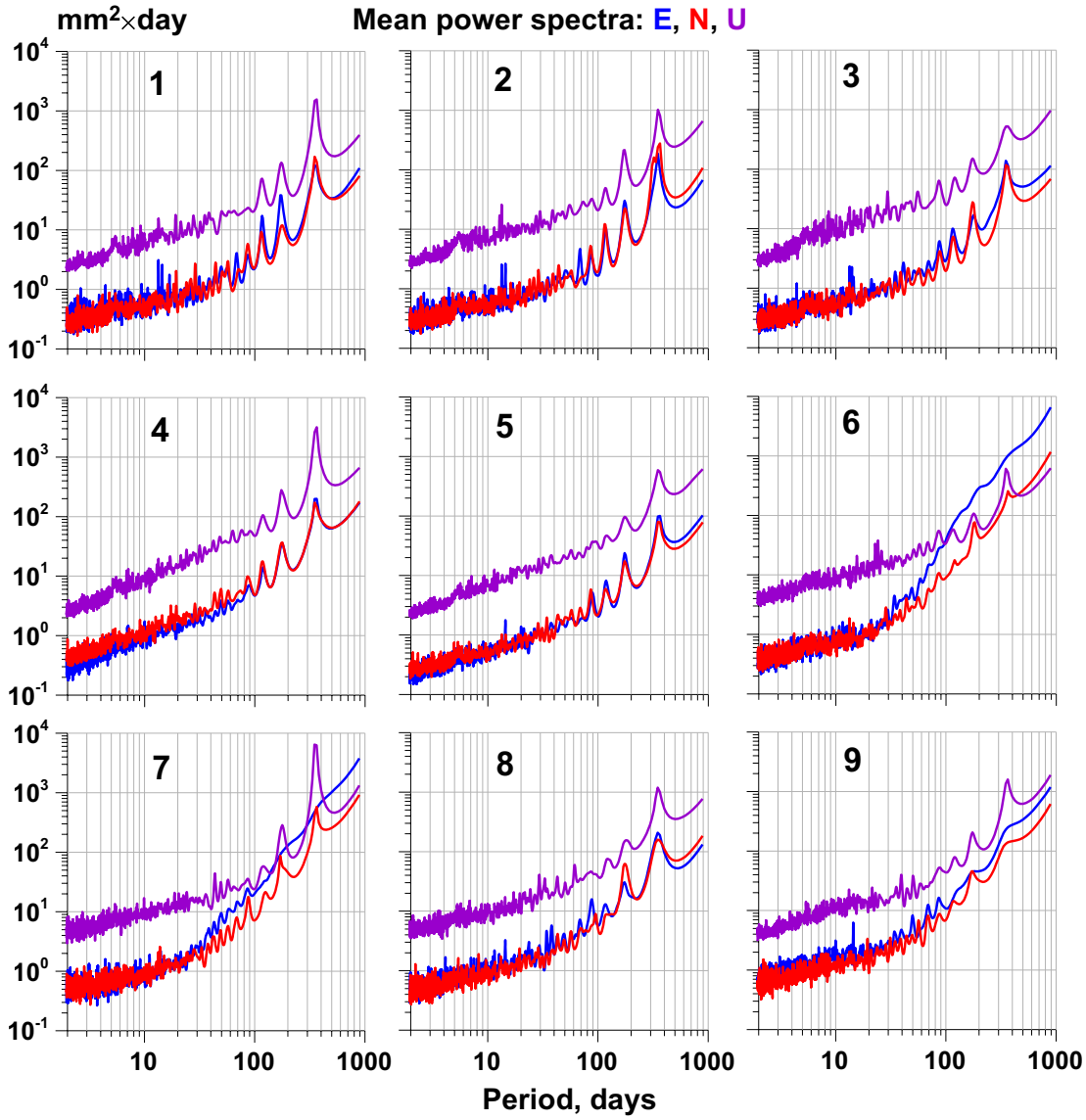

Fig. 5 Graphs of mean power spectra for the nine domains from Table 1. Blue lines present spectra of E records, red lines—N-records, and purple lines—U records

For more precise investigation of this effect, let us average values (4) within each time window by all the frequency values:

$$\rho(\tau) = \sum_{\omega} \varphi(\tau, \omega)/N_{\omega}, \tag{7}$$

where N_{ω} is the number of all discrete frequency ω values for which spectral matrices are calculated. Usually, one takes $N_{\omega} = L/2$.

Fisher's ratio

In Fig. 7, the averaged values $\rho(\tau)$ of mean coherence are presented by blue lines. It is clearly seen that these averaged values have a rather fast change within some time intervals which have right-hand end at the vicinity of beginning of 2011. It is necessary to find change points corresponding to maximum increasing of the mean squared coherence using some quantitative method. For this purpose, we used a method which is based on the Fisher's criterion from analysis of variance (ANOVA) (Rao 1965).

Let us calculate the general mean value of $\rho(\tau)$ as $\bar{\rho}_0 = \sum_{\tau=1}^{N_\tau} \rho(\tau)/N_\tau$ where N_τ is the general number of time

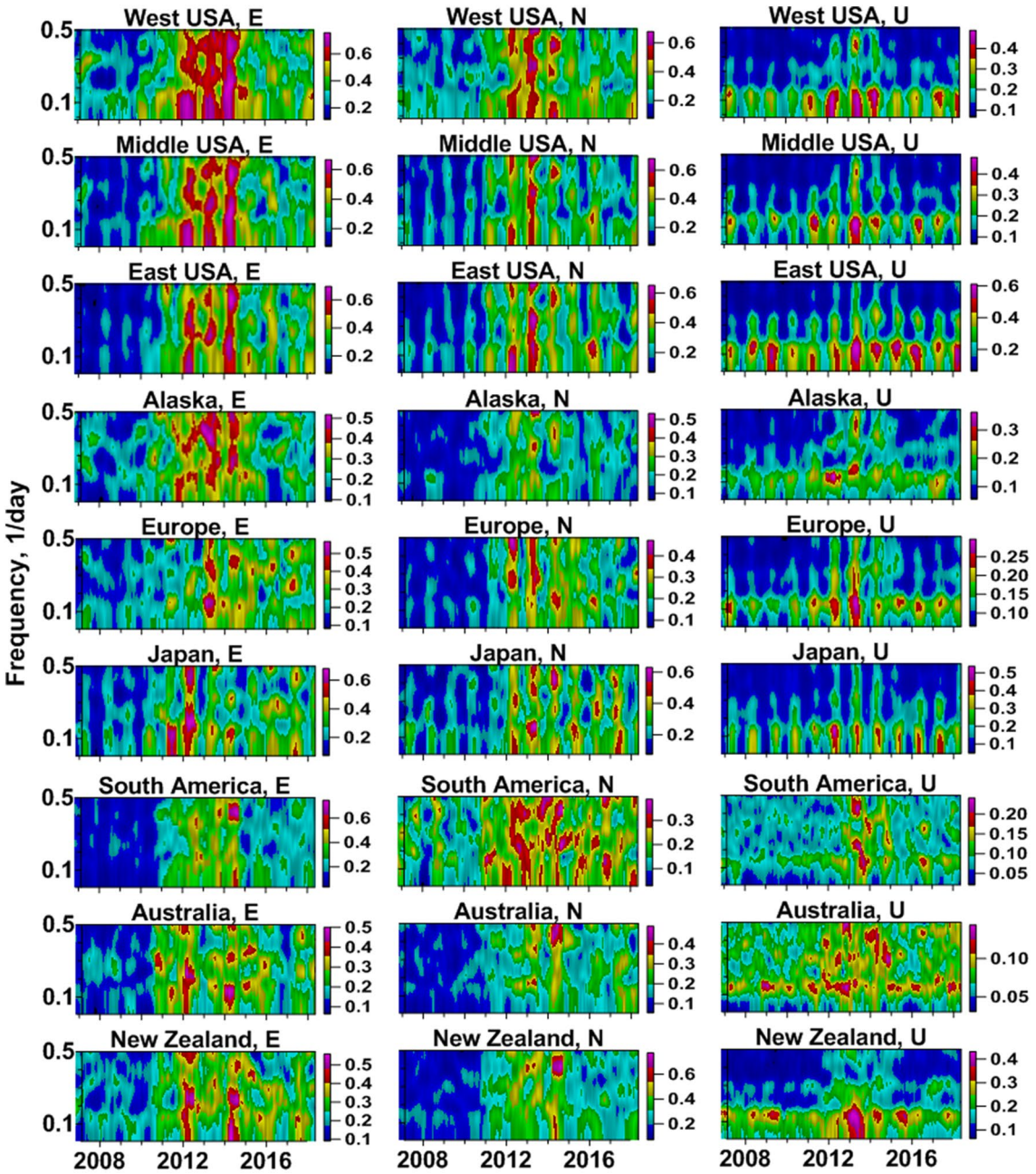

Fig. 6 Time–frequency diagrams of mean squared coherence for all nine domains and for all three components of GPS time series in dependence on the right-hand end of moving the time of the length 182 days with mutual shift 28 days

windows and mean values of $\rho(\tau)$ from left and right sides of the probe time moment τ_C of the change point: $\bar{\rho}_1 = \sum_{\tau=1}^{\tau_C} \rho(\tau)/\tau_C$ and $\bar{\rho}_2 = \sum_{\tau=\tau_C+1}^{N_\tau} \rho(\tau)/(N_\tau - \tau_C)$. Change point τ_C is found from the condition:

$$F(\tau_C) = S_1^2(\tau_C)/S_2^2(\tau_C) \to \max_{\tau_C}, \tag{8}$$

where

$$S_1^2(\tau_C) = \tau_C \cdot (\bar{\rho}_1 - \bar{\rho}_0)^2 + (N_\tau - \tau_C) \cdot (\bar{\rho}_2 - \bar{\rho}_0)^2,$$

$$S_2^2(\tau_C) = \left(\sum_{\tau=1}^{\tau_C} (\rho(\tau) - \bar{\rho}_1)^2 + \sum_{\tau=\tau_C+1}^{N_\tau} (\rho(\tau) - \bar{\rho}_2)^2 \right) / (N_\tau - 2) \tag{9}$$

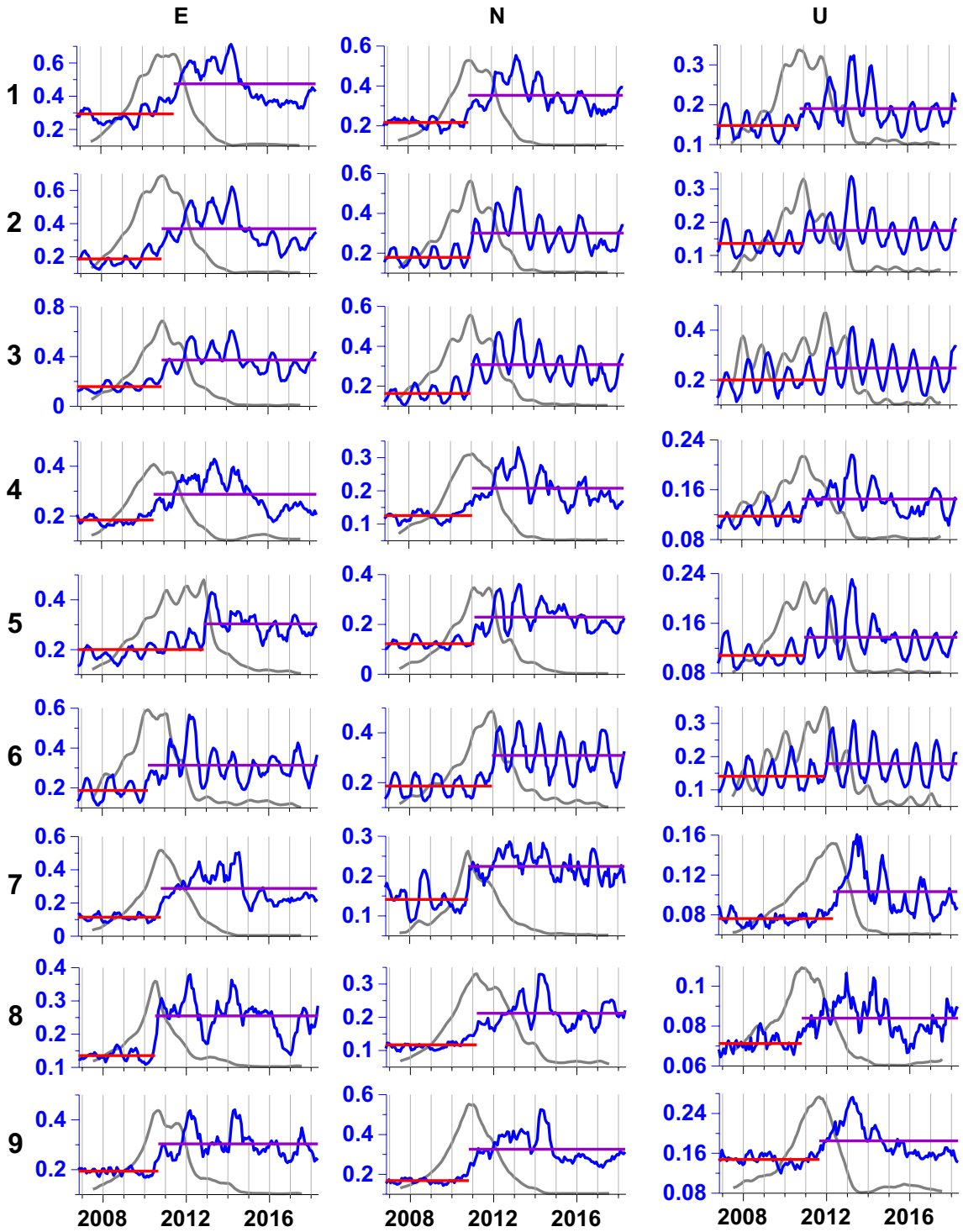

Fig. 7 Graphs of the averaged values $\rho(\tau)$ of mean coherence for all nine domains and for all three components of GPS time series (blue lines). Graphs of Fisher's ratio are presented by grey lines. Mean values of $\rho(\tau)$ from left and right sides of change points defined from maximum of Fisher's ratio (read and purple horizontal lines). Each row of plots corresponds to one of the domains of Table 1, whereas each column corresponds to different components of GPS time series. All graphs are given in dependence on the right-hand end of the moving time window of the length 182 days with mutual shift of 28 days

Table 2 Values of change points defined from maximum of Fisher's ratio for mean coherence

#	Domain	E	N	U
1	West USA	2011.531	2010.918	2010.841
2	Middle USA	2010.918	2010.994	2010.994
3	East USA	2010.918	2010.994	2012.067
4	Alaska	2010.534	2011.071	2010.918
5	Europe	2012.911	2011.148	2010.994
6	Japan	2010.228	2011.991	2011.991
7	South America	2010.841	2010.841	2012.374
8	Australia	2010.534	2011.224	2010.841
9	New Zealand	2010.688	2010.841	2011.684

are values of the weighted square distance of mean values $\bar{\rho}_1$ and $\bar{\rho}_2$ of two groups of data from the general mean value $\bar{\rho}_0$ and of a weighted sum of square distances of elements within each group from their mean values.

Figure 7 shows the graphs of Fisher's ratio $F(\tau_C)$ by grey lines. The mean values $\bar{\rho}_1$ and $\bar{\rho}_2$ from left and right sides of change points, which are defined from condition (8), are presented by red and purple horizontal lines. Table 2 contains values of change points τ_C for all domains of the Table 1 and for all components of GPS time series.

Besides averaging over frequency values in (7), we can perform averaging over all positions of time windows:

$$\psi(\omega) = \sum_{\tau} \varphi(\tau, \omega)/N_{\tau}. \tag{10}$$

Graphs of functions (10) for all domains are presented in Fig. 8. We can notice that there are a lot of individual peculiarities in the behavior of functions $\psi(\omega)$ in different regions, but there is one common characteristic: periods 7–9 days provide a maximum of coherence for all domains and for all components of GPS time series.

Time–frequency principal components

Let us try to extract the most common peculiarities in the behavior of the two-dimensional functions $\varphi(\tau, \omega)$ by applying the principal components approach (Jolliffe 1986). Let $\varphi_\alpha(\tau, \omega)$ be functions (4) for domains with numbers $\alpha = 1, ..., m_D = 9$ of Table 1. The first step in applying principal components method is preliminary normalizing:

$$\varphi'_\alpha(\tau, \omega) = (\varphi_\alpha(\tau, \omega) - \mu_\alpha)/\sigma_\alpha, \tag{11}$$

where

$$\mu_\alpha = \sum_{\tau,\omega} \varphi_\alpha(\tau, \omega)/(N_\tau \cdot N_\omega), \quad \sigma_\alpha^2 = \sum_{\tau,\omega} (\varphi_\alpha(\tau, \omega) - \mu_\alpha)^2/(N_\tau \cdot N_\omega) \tag{12}$$

are sample estimates of mean and variance of $\varphi_\alpha(\tau, \omega)$. Elements of the covariance matrix of normalized functions $\varphi'_\alpha(\tau, \omega)$ are defined by the formula:

$$C_{\alpha\beta} = \sum_{\tau,\omega} \varphi'_\alpha(\tau, \omega) \cdot \varphi'_\beta(\tau, \omega)/(N_\tau \cdot N_\omega), \quad \alpha, \beta = 1, ..., m_D \quad , \tag{13}$$

and a first-principal component of functions $\varphi_\alpha(\tau, \omega)$ is calculated by the following formula:

$$p(\tau, \omega) = \sum_{\alpha=1}^{m_D} c_\alpha \cdot \varphi'_\alpha(\tau, \omega), \tag{14}$$

where c_α are components of the eigenvector of the matrix $(C_{\alpha\beta})$ corresponding to its maximum eigenvalue. Similar to (7) and (10), we can define values which are obtained by averaging (14) over all frequency values and positions of time windows separately:

$$r(\tau) = \sum_{\omega} p(\tau, \omega)/N_\omega, \quad g(\omega) = \sum_{\tau} p(\tau, \omega)/N_\tau. \tag{15}$$

Figure 9a1–c1 presents time–frequency diagrams of the first-principal components $p(\tau, \omega)$ for the three components of GPS time series. Plots in blue lines at Panels (a2–c2) present graphs of functions $r(\tau)$; the grey lines denote graphs of Fisher's ratio (8) for $r(\tau)$, and the red and purple horizontal lines are the mean values from left and right sides of change points defined from a maximum of Fisher ratio. Figure 9a3–c3 presents frequency-dependent first-principal components $g(\omega)$.

Change points for horizontal components E and N which are obtained from the maximum of Fisher's ratio in Fig. 6a2, b2 as 2010.751 and 2011.057. For the vertical component U, the Fisher's ratio in Fig. 6c2 has two local maximums which differ at a very slight value at the change points 2011.057 and 2011.977. Periods corresponding to maximums of frequency-dependent first-principal components $g(\omega)$ at Fig. 6a3–c3 are equal to 7–9 days for all the components of GPS time series.

Mean absolute correlations

Along with the previously used spectral approach, a method based on the calculation of all pairwise correlation coefficients with subsequent averaging of their absolute values can be applied. The correlation method is much simpler than the method based on the use of pairwise quadratic coherences, but its drawback is the lack of information about the periods to which the maximal coherences correspond (Figs. 8,

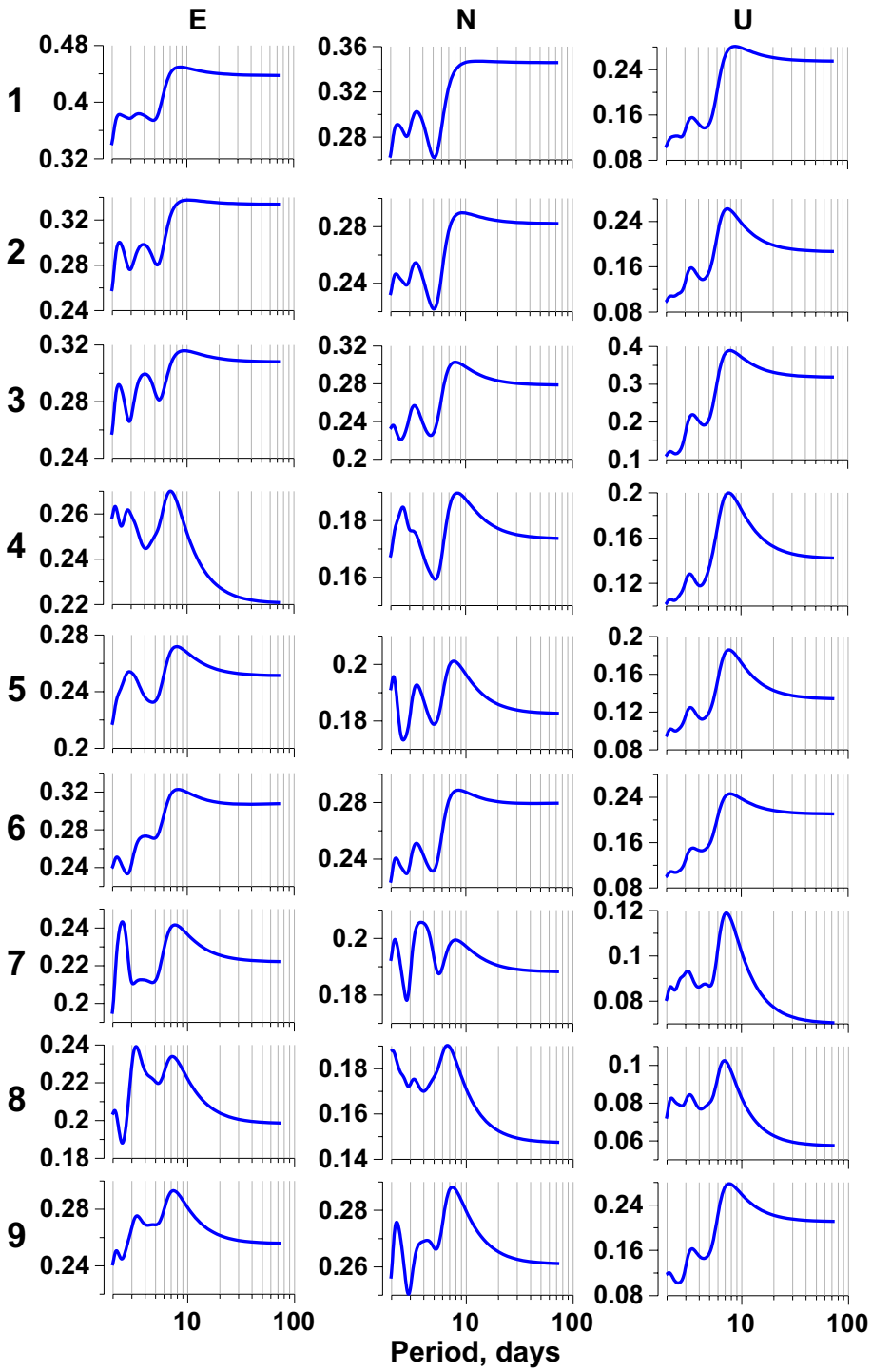

Fig. 8 Frequency-dependent mean coherence $\psi(\omega)$ after averaging over all time windows for all nine domains and for all three components of GPS time series. Each row of plots corresponds to one of the domains from Table 1, whereas each column corresponds to different components of GPS time series

9a3–c3). Nevertheless, we use it, as well. To do this, in a moving time window of the length 182 days for each region and for each GPS time series component, we calculate all the various pairwise correlation coefficients between increments and average their absolute values. As a result, we obtain changes in the mean absolute correlation measure, to which we can apply the method of determining the significant change in the mean, based on the use of the Fisher's ratio.

The results of such estimates are presented in Fig. 10 which is similar to the Fig. 7. The values of correlations

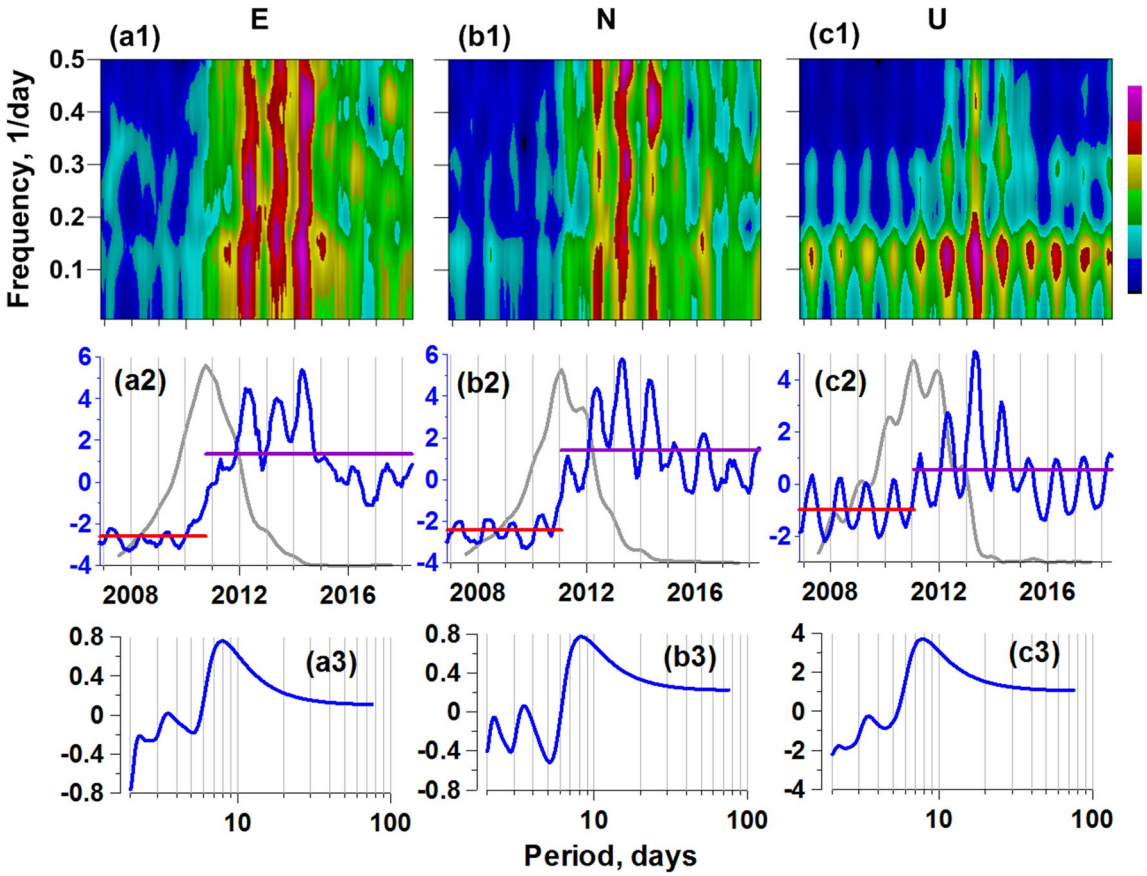

Fig. 9 Time–frequency diagrams (**a1**–**c1**) present the first-principal components computed from mean squared coherence time–frequency diagrams from all nine domains for three components of GPS time series. Graphs (**a2**–**c2**) by blue lines present first-principal components after averaging over all frequency values; grey lines—graphs of Fisher's ratio; red and purple horizontal lines—mean values from left and right sides of change points defined from the maximum of Fisher's ratio. All graphs at (**a1**–**c1**) and (**a2**–**c2**) are given in dependence on the right-hand end of the moving time window of the length 182 days. Graphs (**a3**), (**b3**), and (**c3**) give frequency-dependent first-principal components after averaging over all time windows; periods correspond to maximum values—7–9 days

in Fig. 10 are higher compared to Fig. 7 due to the fact that Fig. 7 presents mean squared coherence, whereas Fig. 10 represents mean absolute correlations. The results of the detection of change points from Fig. 10 are presented in Table 3 which is similar to Table 2. We can notice that time moments are approximately the same.

Finally, let us apply the principal component approach to curves of mean absolute correlations corresponding to different components of the GPS time series. The results are presented in Fig. 11 which is similar to Fig. 9a2–c2.

Results presented in Figs. 10 and 11 and Table 3 show that the simpler method based on mean absolute correlations provides practically the same results as the method of mean squared coherence except for the information about periods.

One of the hypotheses of the reasons for a rather fast increase in the global coherence or correlations of the high-frequency components of the daily GPS time series is the change in some technical conditions for the formation of these data. Without denying the possibility of such a cause, however, it should be noted that, in this case, there would be an abrupt synchronous change in the correlation properties of time series for all the considered regions and for all components. A closer look at the graphs in Figs. 7 and 10 shows that an abrupt change occurs only for some regions and some components; for example, for the graphs N2, N3, N6, N7, E8 in Fig. 7 and N2, N3, N5, N6, N9, E8, E9 in Fig. 10. For other variants of combining regions and components, this growth is fast, but it could not be called a jump. In Figs. 9 and 11 for the principal components, we generally do not observe an abrupt change in the shape of the jump; there is a rapid change in the mean level, which lasts approximately 2 years, 2010–2012. Moreover, after a significant increase in

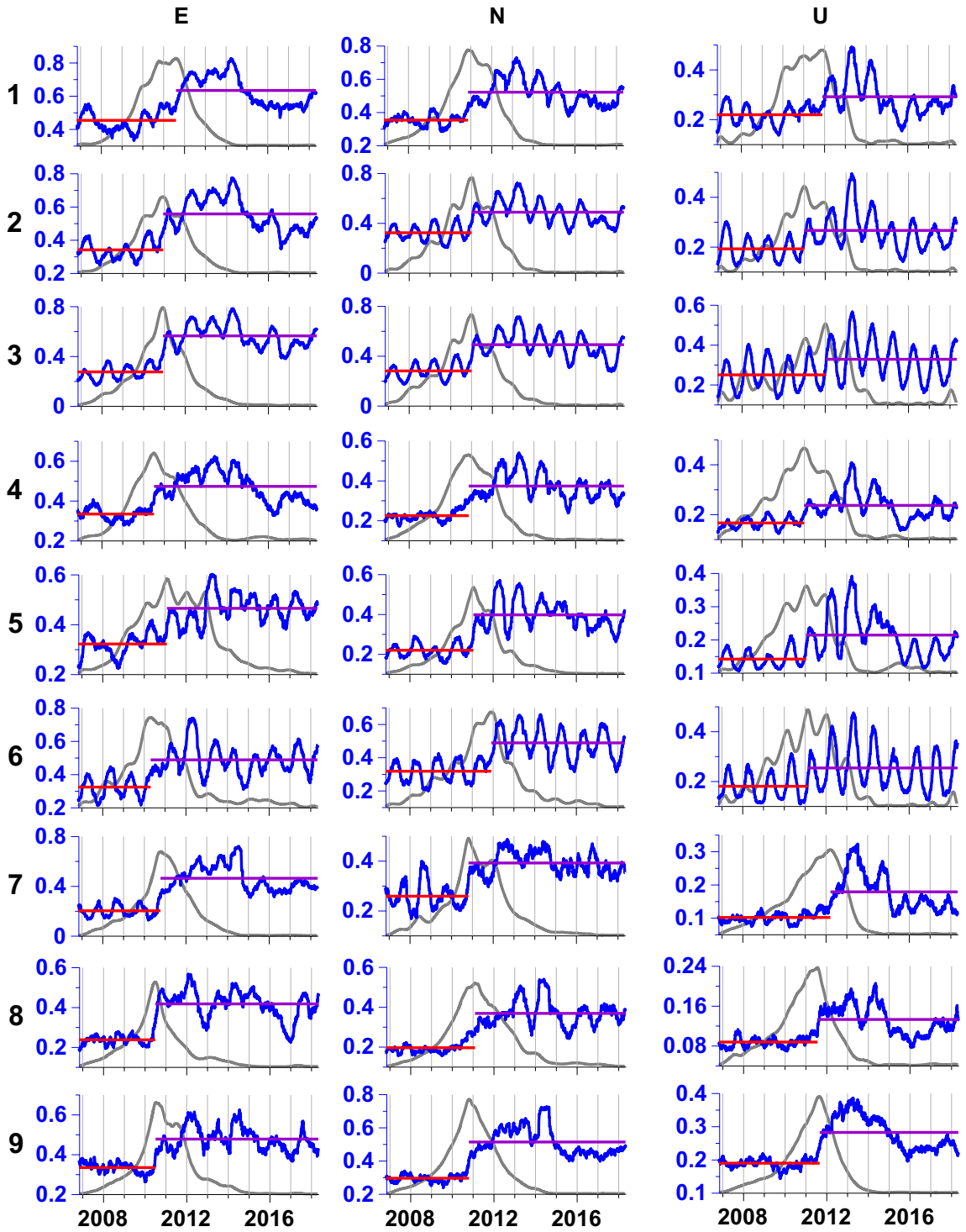

Fig. 10 Graphs of averaged values of absolute by-pair correlation coefficients for all nine domains and for all three components of GPS time series are presented by blue lines in dependence on right-hand end of moving time of the length 182 days; grey lines give graphs of Fisher ratio; red and purple horizontal lines—mean values of mean absolute correlations from left and right sides of change points defined from maximum of Fisher ratio. Each row of plots corresponds to one of the domains from Table 1, whereas each column corresponds to different components of GPS time series

Table 3 Values of change points defined from maximum of Fisher's ratio for mean absolute correlations

#	Domain	E	N	U
1	West USA	2011.625	2010.896	2011.929
2	Middle USA	2010.973	2011.033	2011.022
3	East USA	2010.970	2011.030	2012.055
4	Alaska	2010.534	2010.896	2011.016
5	Europe	2011.118	2011.085	2011.077
6	Japan	2010.340	2011.945	2011.159
7	South America	2010.808	2010.844	2012.243
8	Australia	2010.526	2011.123	2011.592
9	New Zealand	2010.540	2010.833	2011.693

Change points correspond to the right-hand end of the moving time window of the length 182 days

the average level, starting in 2014, we see a smooth decline with the release to some new level, significantly exceeding the level until 2010.

Thus, the revealed effect of changes in global GPS correlations is inherently a certain process, including transitional stages and sufficiently extended in time. To get additional information about the time structure of this process, let us calculate the average values of the standard deviation of GPS time series increments and the mean values of the absolute values of pairwise correlations for all 1191 stations whose positions are shown in Fig. 1. Calculations will be performed in a sliding time window of 182 days. The results of these calculations are shown in Fig. 12.

It can be seen from the graphs in Fig. 12 that changes in the mean absolute correlations and standard deviations correlate well with each other. Thus, the cause of increasing global coherence and correlations of GPS noise can be a global increase in the average noise intensity.

Conclusion

It should be noted that all the time moments presented in Tables 2 and 3 refer to the right end of a moving time window of the length 182 days. That is, changes in the properties of coherence or correlation of time series measured at different stations, leading to a rather sharp change in the average level of synchronization measures, occur at time intervals of 6 months in length before the time points determined by the Fisher's ratio.

The main issue that arises in interpreting the results of this study is the cause of the rapid global increase in the synchronization measure in 2010–2011. Of course, we would like this increase to be due to the internal dynamics of the planet earth. Another explanation may relate this effect to changes in the technical conditions for conducting GPS measurements. One can only propose some speculative theories and compare the effect obtained with the synchronization of other geophysical observations. In Lyubushin (2014, 2015, 2018), the effect of the continued increase in the synchronization of parameters of global low-frequency seismic noise after the mega-earthquake in Sumatra in late 2004 was discovered, after which the activation of the strongest earthquakes around the world began. It can be assumed that the detected effect of increasing the synchronization of GPS readings is somehow connected with the general process of synchronizing the earth's own noise.

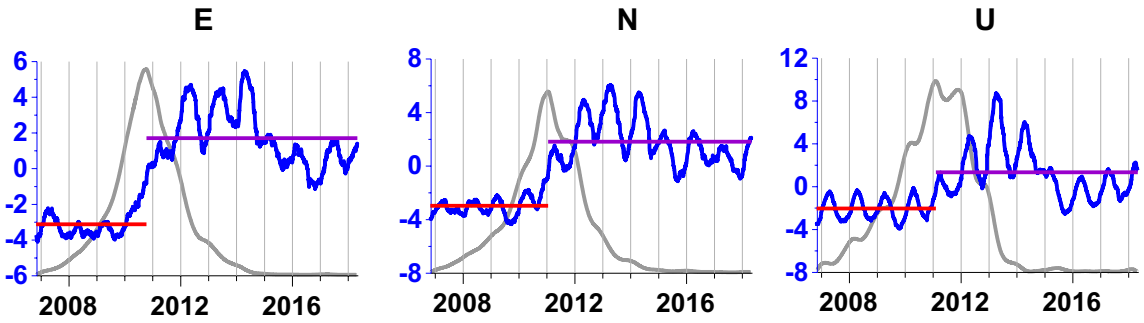

Fig. 11 Graphs of first-principal components of mean absolute correlations computed from all nine domains for three components of GPS time series are presented by blue lines; grey lines give graphs of Fisher ratio; red and purple horizontal lines—mean values from left and right sides of change points defined from maximum of Fisher's ratio. Change points from maximum of Fisher's ratio: for E—2010.808, for N—2011.074, and for U—2011.129. All graphs are given in dependence on the right-hand end of the moving time window of the length 182 days

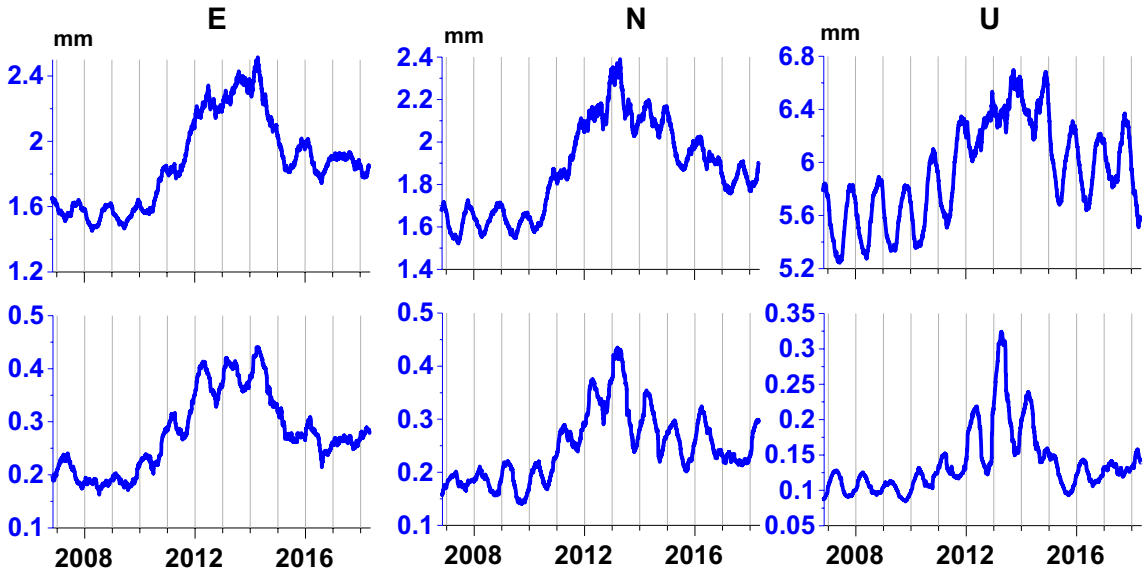

Fig. 12 Graphs of mean values of standard deviations are presented at the top panel. Standard deviations were calculated within moving time window of the length 182 days for daily time series for components E, N, and U from all 1191 GPS stations, which are presented in Fig. 1. Bottom panel presents graphs of mean values of absolute by-pair correlations between records from these GPS stations calculated within moving time windows of the same length. All graphs are given in dependence on the right-hand end of the moving time window of the length 182 days

Acknowledgements The author is grateful to the Indiana University Bloomington and University of Nevada, Reno for providing free access to three-component GPS daily time series from the global network consisting of 10590 permanent stations all over the world. This work was supported by the Russian Foundation for Basic Research (Project no. 18-05-00133).

References

Beavan J (2005) Noise properties of continuous GPS data from concrete pillar geodetic monuments in New Zealand and comparison with data from US deep drilled braced monuments. J Geophys Res 110:B08410. https://doi.org/10.1029/2005JB003642

Blewitt G, Lavallee D (2002) Effects of annual signal on geodetic velocity. J Geophys Res 107(B7):2145. https://doi.org/10.1029/2001JB000570

Bock Y, Melgar D, Crowell BW (2011) Real-time strong-motion broadband displacements from collocated gps and accelerometers. Bull Seismol Soc Am 101(6):2904–2925. https://doi.org/10.1785/0120110007

Bos MS, Fernandes RMS, Williams SDP, Bastos L (2008) Fast error analysis of continuous GPS observations. J Geod 82(3):157–166. https://doi.org/10.1007/s00190-007-0165-x

Bos MS, Bastos L, Fernandes RMS (2010) The influence of seasonal signals on the estimation of the tectonic motion in short continuous GPS time-series. J Geodyn 49(3–4):205–209. https://doi.org/10.1016/j.jog.2009.10.005

Box GEP, Jenkins GM, Reinsel GC, Ljung GM (2015) Time series analysis—forecasting and control, 5th edn. Wiley, Hoboken

Caporali A (2003) Average strain rate in the Italian crust inferred from a permanent GPS network—I. Statistical analysis of the time-series of permanent GPS stations. Geophys J Int 155:241–253. https://doi.org/10.1046/j.1365-246X.2003.02034.x

Chen Q, van Dam T, Sneeuw N, Collilieux X, Weigelt M, Rebischung P (2013) Singular spectrum analysis for modeling seasonal signals from GPS time series. J Geodyn 72:25–35. https://doi.org/10.1016/j.jog.2013.05.005

Filatov DM, Lyubushin AA (2017) Fractal analysis of GPS time series for early detection of disastrous seismic events. Phys A 469(1):718–730. https://doi.org/10.1016/j.physa.2016.11.046

Goudarzi MA, Cocard M, Santerre R, Woldai T (2013) GPS interactive time series analysis software. GPS Solut 17(4):595–603. https://doi.org/10.1007/s10291-012-0296-2

Hackl M, Malservisi R, Hugentobler U, Jiang Y (2013) Velocity covariance in the presence of anisotropic time correlated noise and transient events in GPS time series. J Geodyn 72:36–45. https://doi.org/10.1016/j.jog.2013.08.007

Hamilton JD (1994) Time series analysis. Princeton University Press, Princeton

Huber PJ, Ronchetti EM (2009) Robust statistics, 2nd edn. John Wiley, Hoboken

Jolliffe IT (1986) Principal component analysis. Springer, Berlin

Khelif S, Kahlouche S, Belbachir MF (2013) Analysis of position time series of GPS-DORIS co-located stations. Int J Appl Earth Obs Geoinf 20:67–76. https://doi.org/10.1016/j.jag.2011.12.011

Langbein J (2008) Noise in GPS displacement measurements from Southern California and Southern Nevada. J Geophys Res 113:B05405. https://doi.org/10.1029/2007JB005247

Langbein J, Johnson H (1997) Correlated errors in geodetic time series, implications for time-dependent deformation. J Geophys Res 102(B1):591–603. https://doi.org/10.1029/96JB02945

Li J, Miyashita K, Kato T, Miyazaki S (2000) GPS time series modeling by autoregressive moving average method, application to the crustal deformation in central Japan. Earth Planets Space 52:155–162. https://doi.org/10.1186/BF03351624

Lyubushin AA (2014) Analysis of coherence in global seismic noise for 1997–2012. Izv Phys Solid Earth 50(3):325–333. https://doi.org/10.1134/S1069351314030069

Lyubushin AA (2015) Wavelet-based coherence measures of global seismic noise properties. J Seismol 19(2):329–340. https://doi.org/10.1007/s10950-014-9468-6

Lyubushin A (2018) Synchronization of geophysical fields fluctuations, chap 6. In: Tamaz C, Luciano T, Vallianatos F (eds) Complexity of seismic time series: measurement and applications. Elsevier, Amsterdam, pp 161–197. https://doi.org/10.1016/B978-0-12-813138-1.00006-7

Lyubushin AA, Yakovlev PV (2016) Entropy measure of stepwise component in GPS time series. Izv Phys Solid Earth 52(1):96–104. https://doi.org/10.1134/S106935131506004X

Mallat S (1999) A wavelet tour of signal processing, 2nd edn. Academic Press, San Diego

Mao A, Harrison CGA, Dixon TH (1999) Noise in GPS coordinate time series. J Geophys Res 104(B2):2797–2816. https://doi.org/10.1029/1998JB900033

Marple SL (Jr) (1987) Digital spectral analysis with applications. Prentice-Hall, Inc., Englewood Cliffs

Rao CR (1965) Linear statistical inference and its applications. John Wiley, London

Teferle FN, Williams SDP, Kierulf HP, Bingley RM, Plag HP (2008) A continuous GPS coordinate time series analysis strategy for high-accuracy vertical land movements. Phys Chem Earth Parts A/B/C 33(3–4):205–216. https://doi.org/10.1016/j.pce.2006.11.002

Wang W, Zhao B, Wang Q, Yang S (2012) Noise analysis of continuous GPS coordinate time series for CMONOC. Adv Space Res 49(5):943–956. https://doi.org/10.1016/j.asr.2011.11.032

Williams SDP, Bock Y, Fang P, Jamason P, Nikolaidis RM, Prawirodirdjo L, Miller M, Johnson DJ (2004) Error analysis of continuous GPS time series. J Geophys Res 109(B3):B03412. https://doi.org/10.1029/2003jb002741

Zhang J, Bock Y, Johnson H, Fang P, Williams S, Genrich J, Wdowinski S, Behr J (1997) Southern California permanent GPS geodetic array: error analysis of daily position estimates and site velocities. J Geophys Res 102(B8):18,035–018,055. https://doi.org/10.1029/97JB01380

Alexey Lyubushin is head of the laboratory in the Institute of Physics of the Earth, Russian Academy of Sciences. Research interests include multidimensional signal processing, wavelet analysis, point process statistics, geophysical monitoring, earthquake prediction, seismic hazard assessment, stochastic climate models, and monitoring time series big data analysis.